Slope of short surface waves and deep ocean pressure
Draft 1

W. E. Farrell and J. Berger

June 1, 2020

Contents

1 Introduction **2**

2 Slopes from ACO spectra **2**
2.1 Slopes of the Farrell & Munk H2O model 2
2.2 Slopes of extended surface wave model 4
2.3 Comparisons with Munk's model 5

3 Slopes from OBSANP spectra **6**
3.1 Slopes of the Farrell & Munk H2O model 7
3.2 Slopes of extended surface wave model 7
3.3 Comparisons with Munk's model 8

4 OBSANP spectra and wind speed **9**

Abstract

1 Introduction

Munk (2009) revisited the problem of ocean glitter, first elucidated decades ago by Cox and Munk. Glitter is dominated by cm scale waves, and is known to vary linearly with wind speed, both down wind and across wind.

Fabrice Ardhuin, in a recent SIO seminar on Munk's paper, reawakened WEF's interest in the subject of the relationship between surface slopes and deep pressure, and particularly what might be learned from analysis of OBSANP data. In the following, we take as a given that the Longuet-Higgins theory of acoustic radiation from surface gravity waves is applicable and apply the theory to two new data sets, ACO (Duennebier et al., 2012) and OBSANP (Farrell et al., 2016).

The earlier conclusion is unchanged: if deep ocean pressure pressure in the band 4-20 Hz is interpreted as LH radiation, the slope spectrum has a nonlinear relationship with U.

2 Slopes from ACO spectra

Farrell and Munk (2013) matched deep ocean pressure spectra from H2O data (Duennebier et al., 2002) with a model assuming it to arise from Longuet-Higgins radiation due to the nonlinear interaction of oppositely directed surface gravity waves. The model took the wave spectrum to be (Farrell and Munk, 2013, Eqn 1)

$$F_\zeta(\kappa, U) = \frac{1}{2}\beta\kappa^m + \gamma\exp(aU)\kappa^n \tag{1}$$

with $\beta = .01, m = -4.25, \gamma = 1.06 \times 10^{-7}, \alpha = .31, \text{and } n = -2.15.$

From the theory of L-H radiation, the wave spectrum at the surface is related to the pressure at twice the frequency at depth by (Farrell and Munk, 2013, Eqn A11)

$$F_p(\omega) = \left[\frac{\pi}{8}\left(\frac{\rho}{c}\right)^2 \omega_A^6 \frac{\kappa_S}{v(\kappa_S)}\right] F_\zeta^2(\kappa_S) R_B^2 I_\kappa \tag{2}$$

In (2) we take $R_B = 1$. The overlap integral, I_κ, is a measure of the directionality of the wave spectrum. For low frequencies and strong winds, the wave field is essentially isotropic and $I = 1/(2\pi)$. For low frequencies and moderate winds, a model for I(U) has been proposed (Farrell and Munk, 2010). In the following we assume, provisionally, that $I = 1/(2\pi)$ at high frequencies. We note, however, that high frequency Aloha spectra were interpreted as evidence of a variable overlap integral (Duennebier et al., 2012, Fig 12).

Equation (2) holds for a bottomless ocean. In the real ocean, the bottom increases the pressure by a few dB over our frequency range. We continue to seek a good Green's function for the OBSANP location so the bottom interaction can be deconvolved.

2.1 Slopes of the Farrell & Munk H2O model

Spectra of deep sea pressure recorded on the Aloha Cabled Array (Duennebier et al., 2012) are reasonably fit by the H2O model for frequencies less than 15 Hz if γ is simply doubled to

2.0×10^{-7} (Fig. 1). The flaring above 40 radians/m in the left panel is due to the second U-dependent term dominating the first, and the doubling in the coefficient γ is a consequence of the winds over ACO being stronger than over H2O during the analyzed epochs. The upward curvature in pressure above 10 Hz in the right panel is due to the dominance of surface tension, the cubic term in the dispersion dispersion relation

$$\omega^2 = g\kappa \left(1 + (\kappa/373)^2\right)^2 \tag{3}$$

The linear and cubic term are equal at $f_{wave} = 13.6$ Hz, or $f_{pressure} = 27$ Hz. The effect enters the pressure expression (2) through the wave number to group velocity ratio, κ/ν.

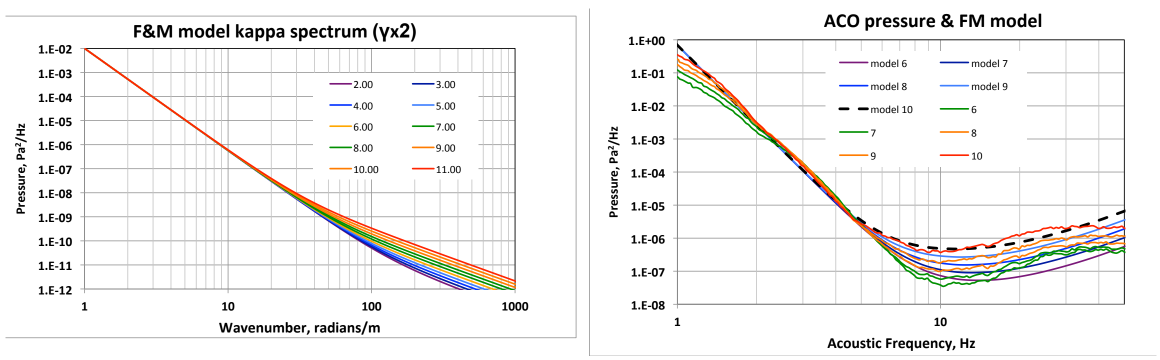

Figure 1: (Left) model wave number spectra for the two element model defined by (1) but with γ doubled from the the value given for (1). (Right) The ACO pressure spectra overlain by model pressure spectra calculated by applying (2) to the wave number model shown in the left.

For glitter analyses it is the wave slope spectrum, not the elevation spectrum, that governs the physics. As detailed in Munk (2009, Section 5.1), the slope spectrum is k^3 times the one-dimensional elevation spectrum. Thus, from model (1), the slope spectrum (following Munk in using "m" for slope) is

$$F_m(\kappa, U) = \frac{1}{2}\beta\kappa^{m+3} + \gamma \exp(aU)\kappa^{n+3} \tag{4}$$

We continue hypothesizing that the deep pressure is due to L-H radiation from surface gravity waves. In this case the pressure spectrum can be inverted to a gravity wave spectrum using (2). Subsequent multiplication by κ^3 gives the inferred slope spectrum (Fig. 2).

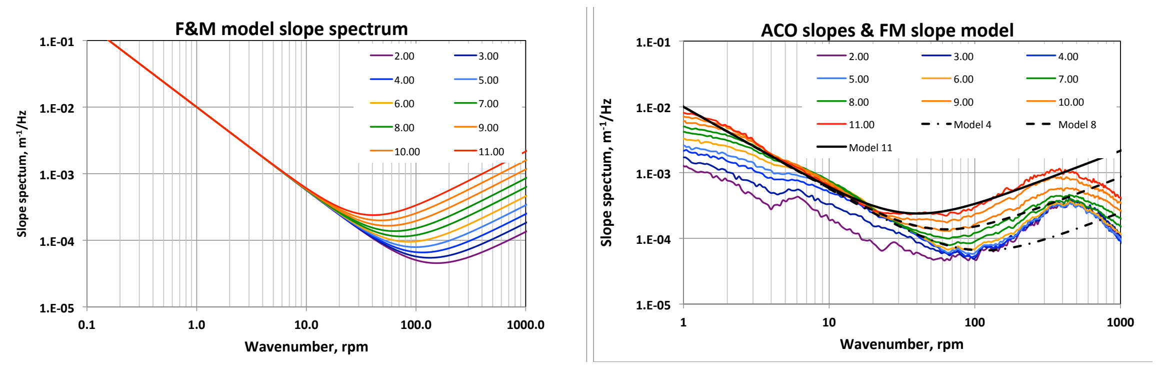

Figure 2: (Left) Model slope spectrum, κ^3 times the data in the left panel of Fig. 1. (Right) The slope spectrum estimated from the ACO data and the L-H radiation assumption, overlain with the model slope spectrum .

2.2 Slopes of extended surface wave model

The two-element wavenumber model gives an imperfect fit to the inferred slope spectra above 50 radians/m and especially above 400 radians/m. To improve the fit at high wavenumbers a four-element model of surface gravity waves was devised as an extension to (1). The model consists of power law segments parameterized to fit the inferred slope spectrum over four distinct frequency regimes. The amplitude parameters were selected to fit the 11 m/s ACO spectrum. The U-dependence is trivial since the slope spectra are sub-parallel for frequencies above 10 Hz (Fig. 3) .

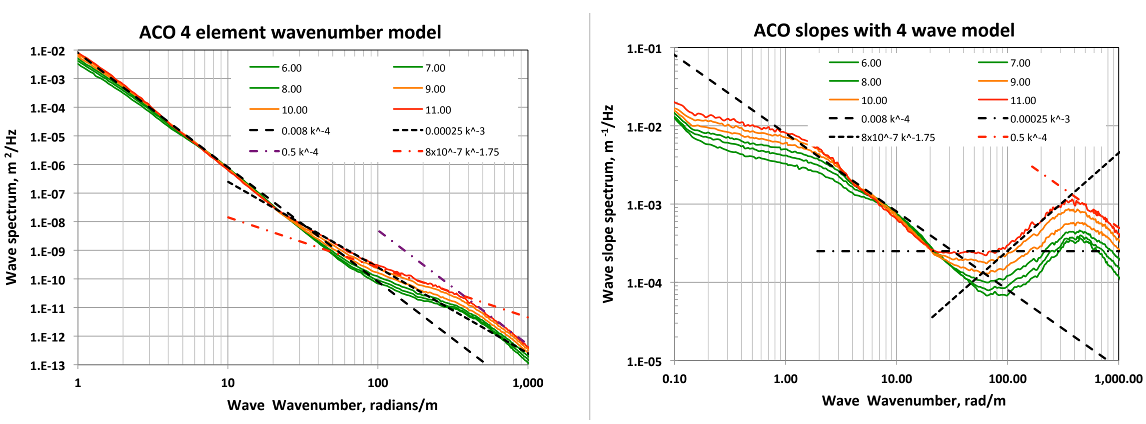

Figure 3: (Left) Wave number spectra of surface gravity waves inferred from ACO pressure spectra (color) overlain with four power law functions (black) with parameters given in the captions. (Rght) Slope spectra derived from the wave spectra shown in left, through multiplication by κ^3.

The extended model fixes the fit to deep pressure at high frequencies (Fig. 4). This improved fit is to be compared with the original model, Fig. 1, right panel.

The variation of the spectra with wind speed is fundamental. Whether one looks at the pressure spectrum or the inferred slope spectrum (Fig. 3), the variation goes as a power of U, not linearly.

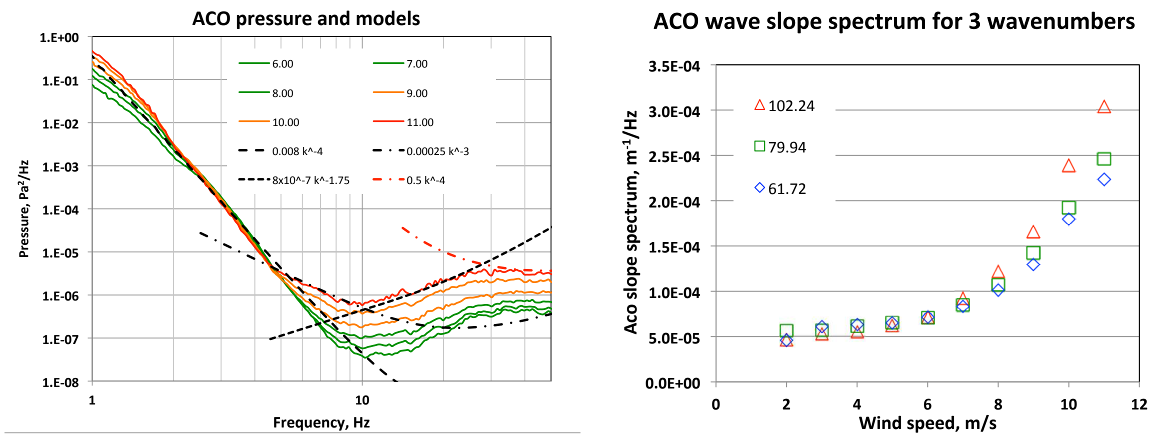

Figure 4: (Left) ACO pressure spectra (color) overlain with pressures of the four-wave model by application of (2). (Right) Inferred slope spectra at three wavenumbers, taken from the data plotted in rhe right panel of Fig. 3.

2.3 Comparisons with Munk's model

From measurements and models of long and short surface gravity waves, Munk (2009) developed a model of the slope spectrum for cyclic frequencies between 10^{-3} and 10^3 cycles/meter. (Fig 5, top). The two panels in the bottom row overlay the two model slope spectra presented above on top of the right portion of Walter's model. My radian wavenumber frequencies have been shifted down by 2π to match Walter's units (there may also be factors of pi in amplitude I've ignored).

Munk's "Hwang short gravities" have a flat slope spectrum, and correspond to my wave number model $.00025 \times \kappa^{-3}$, as plotted in the previous figures. However, it fits the 11 m/s spectra only between 30 and 100 radians/m (5-15 cycle/m), a much smaller range than indicated in the top of Fig. 5.

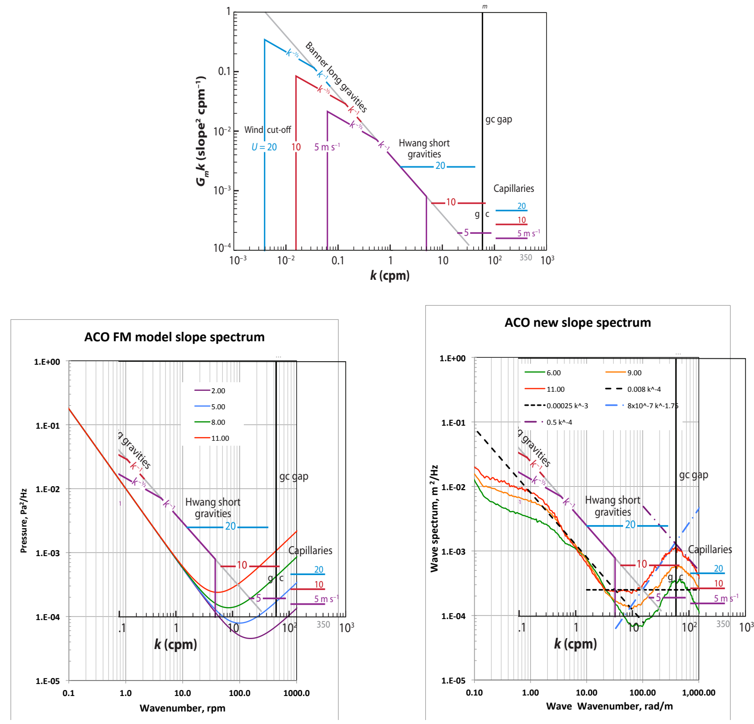

Figure 5: (Top) Fig 15 from Munk (2009) showing the slope spectrum over 4 wave regimes based on analytic fits to experimental data. (Bottom) Slope spectra from fits to the ACO spectrum of the original FM model (right) and the 4 wave model derived above.

3 Slopes from OBSANP spectra

Pressure spectra of OBSANP data were analyzed in the same manner as described above: first following the 2-element F&M model, and secondly by an extended model to lessen the mismatch with data for frequencies 10-40 Hz.. However, with the OBSANP data, the ACO high-frequency roll-over in the spectrum is missing, so the extended OBSANP wave number model has 3 elements, not four.

Other than the the simpler model (3 waves, not 4) the OBSANP analysis is identical to the ACO, so only an abbreviated discussion is given in this draft.

The big difference is the data is our knowledge of overhead winds during the two week OBSNP deployment come from ECMWF weather models, not *in situ* observation. The indirect inference of the P/U relationship for OBSANP is considered briefly in the section following this.

3.1 Slopes of the Farrell & Munk H2O model

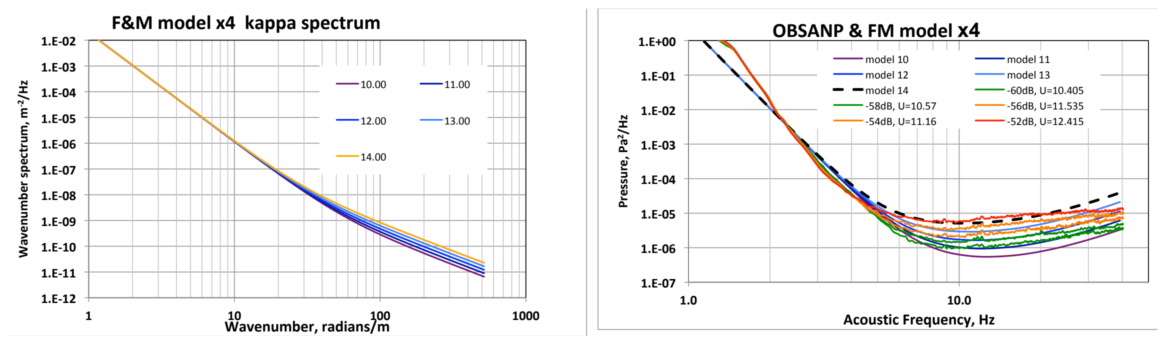

Figure 6: (Left) model wave number spectra for the two element model defined by (1) but with both terms four times larger. (Right) The OBSANP pressure spectra overlain by model pressure spectra calculated by applying (2) to the wave number model shown in the left.

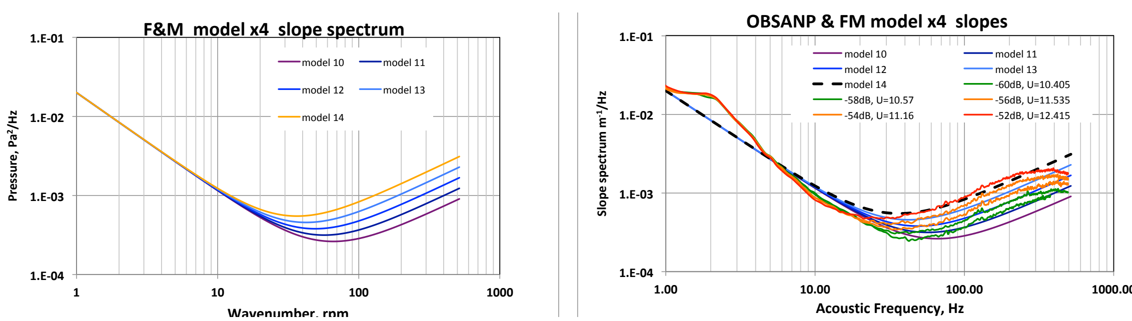

Figure 7: (Left) Model slope spectrum, κ^3 times the data in the left panel of Fig. 6. (Right) The slope spectrum estimated from the OBSANP data and the L-H radiation assumption, overlain with the model slope spectrum .

3.2 Slopes of extended surface wave model

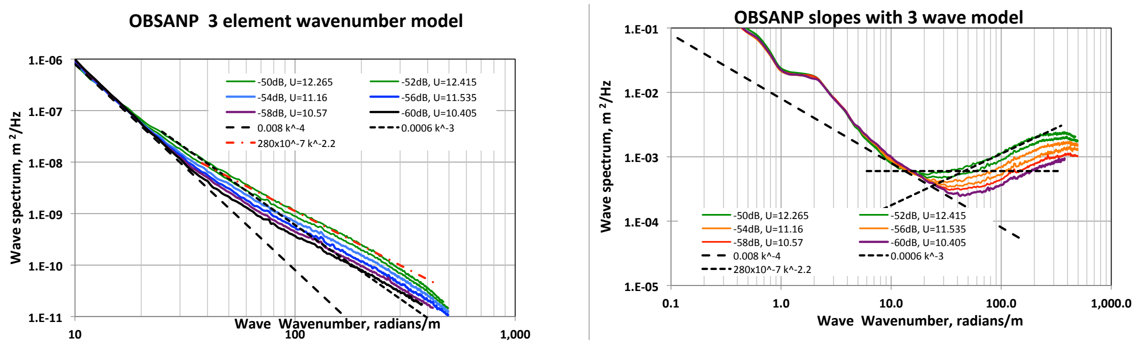

Figure 8: (Left) Wave number spectra of surface gravity waves inferred from OBSANP pressure spectra (color) overlain with three power law functions (black) with parameters given in the captions. (Right) Slope spectra derived from the wave spectra shown in left, through multiplication by κ^3.

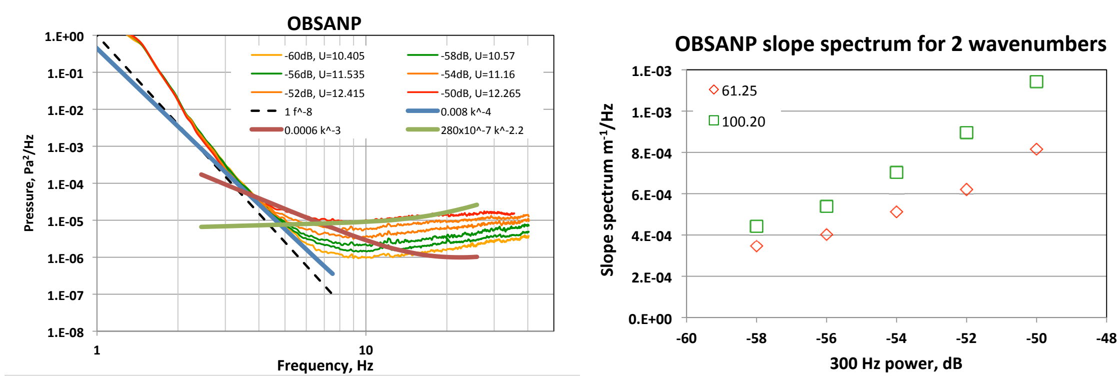

Figure 9: (Left) OBSANP pressure spectra (color) overlain with pressures of the three-wave model by application of (2). (Right) Inferred slope spectra at two wave numbers, taken from the data plotted in the right panel of Fig. 8.

3.3 Comparisons with Munk's model

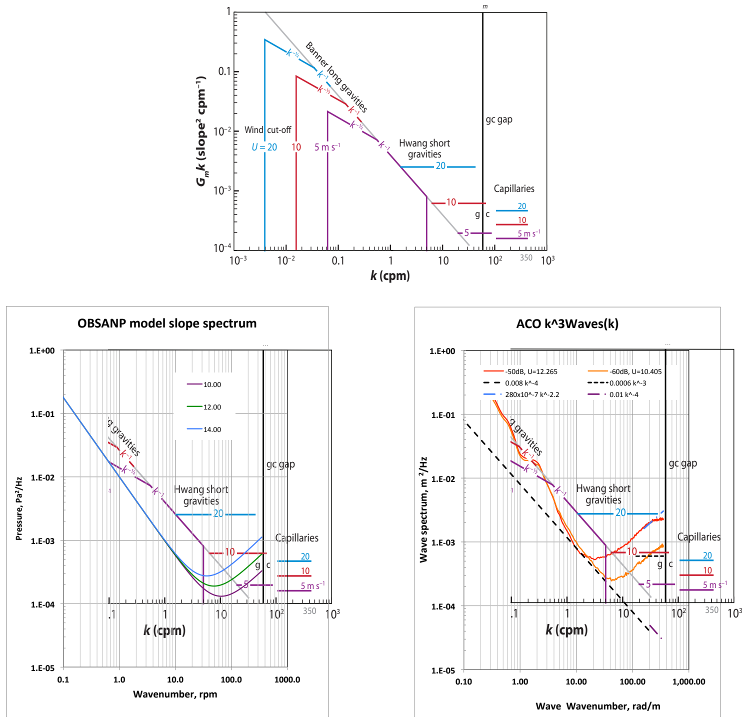

Figure 10: (Top) Fig 15 from Munk (2009) showing the slope spectrum over 4 wave regimes based on analytic fits to experimental data. (Bottom) Slope spectra from fits to the OBSANP spectrum of the original FM model (right) and the 3 wave model derived above.

4 OBSANP spectra and wind speed

Wind speed above the OBSANP location was not directly measured, except when R/B Melville was in the vicinity, but then its acoustic radiation messes the pressure measurements. Jean Bidlot made a number of analyses of OBSANP winds, using the specific location, and interpolating onto hourly estimates. In addition to this approach, there are two indirect approaches that are discussed in what follows. This is very preliminary.

First, there is a great literature on deriving wind from bottom pressure at high frequencies. Thus, high frequency sound can lead to wind, which can be used to interpret the spectrum at low frequencies. Secondly, the ACO P/U data, based on long term measurements north of Oahu, can be mapped reasonably well on the OBSANP spectra.

Fig 11 has averaged OBSANP spectra over two analysis bands.

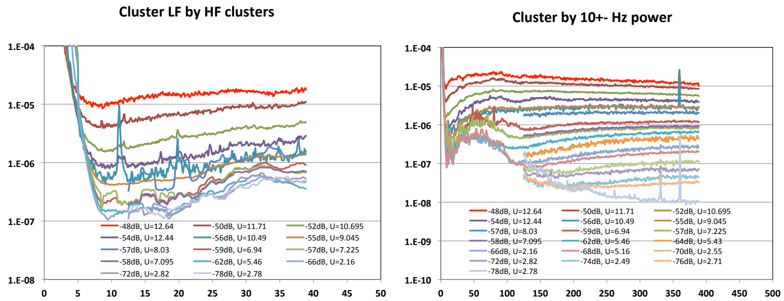

Figure 11: Because of the short observation time, every 10-minute spectrum is important, but many are perturbed by ship interference. (Right) High frequency spectral averages, for 2 dB variations in power. (Left) Averages over the same windows of low frequency spectra.

The ACO results show a non-linear relationship between the 10 Hz spectrum and the 400 Hz spectrum (Fig. 12). This is not new: for the same range of U, the spectral range is greater above the ship hump at 50 Hz than below.

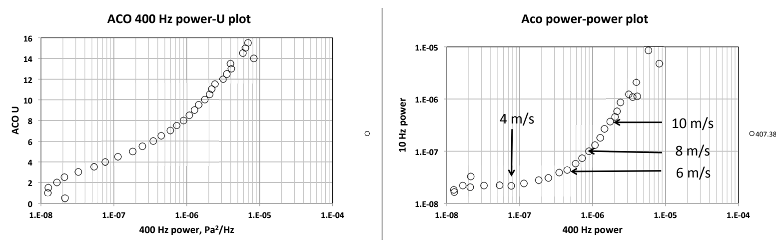

Figure 12: ACO power at 400 Hz plotted against U (left) and against 10 Hz power (right)

Fig 13 has the OBSANP 10Hz to 400 Hz relationship, comparable to the top right panel in Fig 12. Bottom right has power at each frequency versus ECMWF U, and with the ACO relationship displayed in red.

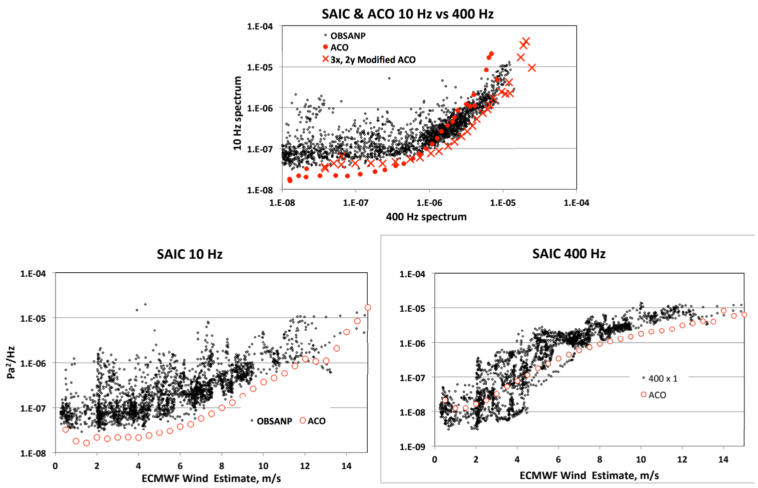

Figure 13: (Top) Scatter plot of OBANP power at 10 Hz vs 400 Hz. The dotted red curve is the ACO equivalent. The red x curve shows an adaption of ACO to more closely conform to the bottom locus of the OBSANP points. (Bottom) Scatter plot of OBSANP spectra against ECMWF U at two frequencies. The red points are from the modified ACO relationship shown as red x curve above.

References

Duennebier, F. K., D. W. Harris, J. Jolly, J. Babinec, D. Copson, and K. Stiffel, 2002: The Hawaii-2 Observatory seismic system. *IEEE J. Oceanic Eng.*, **27 (2)**, 212–217.

Duennebier, F. K., R. Lukas, E. Nosal, J. Aucan, and R. Weller, 2012: Wind, waves, and acoustic background levels at Station ALOHA. *J. Geophys Res.*, **117 (C03017)**, 1–21, doi:10.1029/2011JC007267.

Farrell, W. E., J. Berger, J.-R. Bidlot, M. Dzieciuch, W. Munk, R. A. Stephen, and P. F. Worcester, 2016: Windsea behind a cold front and deep ocean acoustics. *J. Phys. Oceanogr.*, **46 (6)**, 1705–1716, doi:10.1175/JPO-D-15-0221.1.

Farrell, W. E. and W. Munk, 2010: Booms and busts in the deep. *J. Phys. Oceanogr.*, **40**, 2159–2169, doi:10.1175/2010JPO4440.1.

Farrell, W. E. and W. Munk, 2013: Surface gravity waves and their acoustic signatures, 1-30 Hz, on the mid-Pacific sea floor. *J. Acoust. Soc. Am.*, **134 (4) Pt. 2**, 3134–3143, doi:10.1121/1.4818780.

Munk, W., 2009: An inconvenient sea truth: spread, steepness and skewness of surface slopes. *Annual Review of Marine Science*, **1**, 377–415.